PLEASE CITE THIS ARTICLE AS DOI: 10.1063/5.0272922

# Air circulation effects on airborne particles aboard cruise ships

loannis W. Kokkinakis (Ιωάννης Κοκκινάκης) and Dimitris Drikakis (Δημήτρης Δρικάκης)<sup>a)</sup>
Institute for Advanced Modeling and Simulation, University of Nicosia, Nicosia CY-2417, Cyprus

Virus outbreaks on cruise ships pose significant challenges due to their enclosed environments and high passenger densities. Managing these outbreaks has become even more critical as cruise ships have increased in size and passenger capacity. This study uses numerical simulations to investigate the dispersion of airborne respiratory droplets and aerosols within a passenger cabin on a cruise ship, focusing on the angle of the mechanical ventilation jet's influence. Although previous research primarily focused on larger respiratory droplets that quickly settle, this study emphasizes aerosols under 10 micrometers that can remain airborne for extended periods. The findings demonstrate that variations in the inflow angle from the ventilation unit can significantly affect aerosol dispersion. The results show that the travel distance of the larger droplets is more effectively restricted at the larger 75°-degree inlet angle. Smaller droplets with a diameter ranging between 1-10  $\mu$ m and 10-50  $\mu$ m can remain airborne 1.4 meters above ground 20% and 40% longer, respectively. These insights underscore the importance of tailored air circulation strategies to reduce transmission risks in confined spaces, such as cruise ship cabins, highlighting the need for optimized ventilation design to manage infectious disease outbreaks.

# I. INTRODUCTION

Understanding airborne pathogens and mitigating the risk of transmission are particularly pressing issues on cruise ships, where thousands of passengers and crew are confined in enclosed environments. A typical cruise ship accommodates about 2,000 passengers and 800 crew members, while larger vessels can carry more than 5,000 passengers and 2,000 crew. The crowded and confined settings of cruise ships facilitate outbreaks of infectious diseases. This risk is heightened because cruises often last over six days and include group activities that increase interpersonal contact, which can promote the spread of infections. In addition, frequent stops allow passengers and crew personnel to disembark while new individuals board, introducing fresh sources of infections.

Since 2020, the devastating impact of the global COVID-19 pandemic on the cruise industry has been extensively documented. During the pandemic, widely reported outbreaks on cruise ships led to further virus transmission among passengers in their home countries upon their return. By the end of March 2020, all cruises were suspended worldwide, and travel restrictions intensified. Consequently, cruise passengers dropped from 30 million in 2019 to just 6 million in 2020. Estimates indicate that cruise lines suffered losses totaling 77 billion USD between March and September 2020 alone. <sup>2,3</sup>

The persistent threat of infectious diseases on cruise ships is ongoing; see<sup>4</sup> for the recent outbreak of gastrointestinal disease on a cruise ship, where, according to the Centers for Disease Control and Prevention (CDC), about 4.1% of the passengers were affected. The above emphasizes the need to reevaluate and improve maritime health and safety regulations. Optimizing naval architectural and marine engineering systems is crucial in effectively preventing, mitigating, and managing health emergencies in these unique environments.

Although airborne transmission in confined space configurations has been studied for various settings, such as cars<sup>5</sup>,

buses<sup>6</sup>, trains<sup>7</sup>, and elevators<sup>8</sup>, research on this topic for cruise ships is limited. Transmission within passenger cabins has been investigated with mechanistic modeling<sup>9</sup> and data analysis from outbreaks<sup>10</sup>. A recent review on the transmission of COVID-19 on cruise ships indicates that high-occupancy cabins have an increased transmission risk. Still, it does not comment on the ventilation system in the cabin and its potential impact on transmission. <sup>11</sup> Computational fluid mechanics (CFD) studies with ventilation suggestions have been limited to small vessels. <sup>12</sup>

More recently, a typical passenger cabin room was investigated on board a cruise ship to examine the effect of the ventilation rate of a Heating, Ventilation, and Air Conditioning (HVAC) system, corresponding to different air changes per hour (ACHS).<sup>13</sup> They showed that a higher ventilation rate is not always the best strategy to avoid spreading airborne diseases. They proposed using medium flow rates of around 120 m³/h (or 3 ACH) when a cabin is occupied. According to the latest standards for controlling infectious diseases, this is close to the recommended value of 108 m³/h.<sup>14</sup>

Past studies on droplet transmission in enclosed areas included air filtration, purification, and the effectiveness of high-efficiency particulate air filters, which are designed to trap more than 99% particles while maintaining a ventilation rate of 50% fresh air and 50% filtered, ensuring more than 20 air changes in a low ceiling space. <sup>15,16</sup> These studies highlighted that virus transmission remains a concern when people are too close to each other.

A topic that has received less attention in the scientific literature is the effect of air circulation on particle movement, particularly for aerosols. By particles, we refer to liquid droplets as well as aerosols (particles) formed after the complete evaporation of saliva droplets, which can contain up to 1% of other substances (including mucins, proteins, enzymes, mineral salts, and immunoglobulins). The issue is essential for aerosols because they can remain suspended in the air longer. Large droplets typically fall to the ground more quickly due to gravity. Understanding how particles circulate in confined spaces, such as cruise cabins, under varying ventilation conditions, is crucial to reducing pathogen transmission.

Passenger cabins on cruise ships are generally smaller than

a)Electronic mail: Author to whom correspondence should be addressed:

PLEASE CITE THIS ARTICLE AS DOI: 10.1063/5.0272922

Preprint

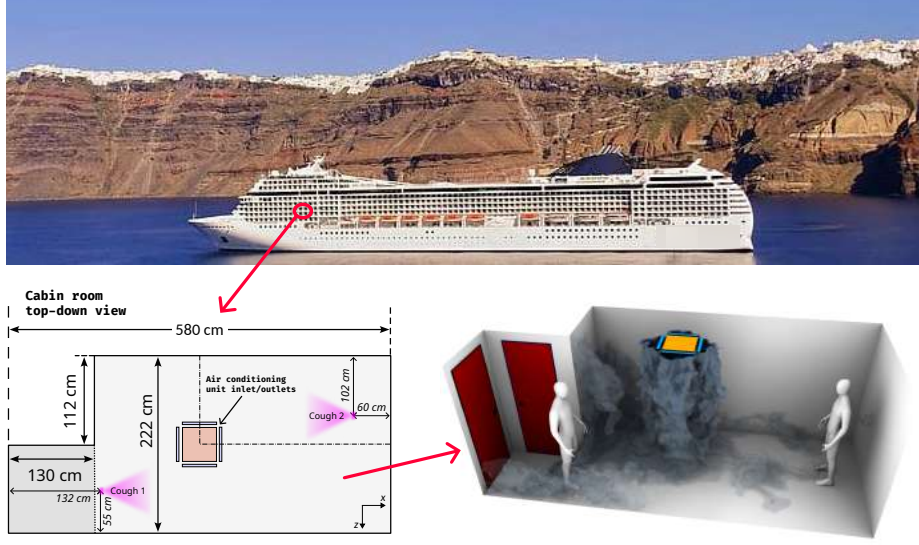


FIG. 1. Illustration of a typical passenger cabin onboard a cruise ship, illustrating the scenario and test case configuration considered.

standard hotel rooms and often have an L-shaped layout to accommodate en-suite bathrooms. Close positioning of air supply and return vents, combined with the smaller size of these cabins, can create complex and sometimes unpredictable airflow patterns. As a result, there can be areas with inadequate ventilation, known as dead zones, and spots where contaminants can accumulate. This can lead to higher concentrations of pollutants within the cabin environment.

Ventilation plays a crucial role in determining the concentration of particles and their distribution within indoor spaces. While ventilation can decrease particle concentration by introducing fresh air into the space and removing particles through the air removal system, it remains unclear how airflow from an air conditioning (a/c) unit affects particle dispersion. Furthermore, the impact of these factors is not well understood when there are two occupants in a cabin, a common scenario on cruise ships. Addressing such issues is vital for establishing norms and regulations to safeguard public health on cruise ships.

Motivated by the challenges outlined above, the present study investigates for the first time the effects of mechanically induced flow circulation on respiratory droplets and aerosols ranging from 1 to 300  $\mu m$  in diameter within a typical passenger cabin room on board a cruise liner occupied by two individuals (Figure 1). Cabins represent some of the narrowest spaces on board ships, meaning that even slight ventilation changes can significantly affect air circulation and passenger comfort. The study's findings indicate that the prediction of particle circulation is not straightforward, revealing that the a/c inflow angle influences (i) particle deposition on

the ground, (ii) airborne dispersion, and (iii) the duration for which aerosols remain suspended in the air. These results can help guide the use of a/c in cruise cabins and, more generally, inform the development of environmental policies and strategies to reduce airborne transmission in indoor settings.

# II. METHODOLOGY

# A. Governing equations

# 1. The Navier-Stokes equations (Eulerian)

The three-dimensional Navier-Stokes (NS) equations for a Newtonian viscous air mixture are considered. For a finite control volume, dV, in the *Eulerian* frame of reference, the multicomponent NS equations can be expressed in the fully conservative (four-equation) form<sup>17</sup> as follows:

Mass:

$$\frac{\partial}{\partial t} \iiint_{V} \rho \, dV = - \oiint_{A} \rho \mathbf{u} \cdot \hat{\mathbf{n}} dA + \iiint_{V} S_{m} \, dV, \qquad (1)$$

Momentum

$$\frac{\partial}{\partial t} \iiint_{V} \rho \mathbf{u} \, dV = - \iint_{A} (\rho \, \mathbf{u} \otimes \mathbf{u} + p \, \mathbf{I} - \tau) \cdot \hat{\mathbf{n}} dA 
+ \iiint_{V} \rho \, (\mathbf{f}_{b} + \mathbf{S}_{u}) \, dV,$$
(2)

PLEASE CITE THIS ARTICLE AS DOI: 10.1063/5.0272922

Preprint 3

Total energy:

$$\begin{split} \frac{\partial}{\partial t} \iiint\limits_{V} \rho \, e_t \, \mathrm{dV} &= - \iint\limits_{A} \left( \mathbf{u} \rho h_t - \mathbf{u} \cdot \boldsymbol{\tau} - \mathbf{q_c} - \mathbf{q_d} \right) \cdot \hat{\mathbf{n}} \mathrm{dA} \\ &+ \iiint\limits_{V} \rho \left( \mathbf{f}_b \cdot \mathbf{u} + \dot{h} + S_h \right) \, \mathrm{dV}, \end{split} \tag{3} \end{split}$$

Species mass:

$$\frac{\partial}{\partial t} \iiint_{V} \rho w_{j} \, dV = - \iint_{A} (\rho w_{j} \mathbf{u} - \mathbf{J}_{j}) \cdot \hat{\mathbf{n}} dA$$

$$+ \iiint_{V} \rho \left( \dot{w}_{j} + S_{w_{j}} \right) \, dV,$$
(4)

where  $\rho$  is the mixture density;  $\mathbf{u}$  is the velocity vector; p is the static pressure;  $\hat{\mathbf{n}}$  is the outward pointing unit normal of a surface element dA of the closed finite control volume dV;  $\mathbf{f}_b$  is an external body force;  $h_t = e_t + p/\rho$  is the total specific enthalpy (per unit mass);  $e_t = e + \mathbf{u} \cdot \mathbf{u}/2$  is the total specific energy;  $e = c_v T$  is the specific internal energy;  $w_j$  is the massfraction of the jth species. We denote T the temperature,  $c_v$  the specific heat capacity at constant volume, and  $\gamma = c_p/c_v$  the heat capacity ratio where  $c_p$  and  $c_v$  are the specific heat capacity at constant pressure and volume, respectively.

The terms  $S_m$ ,  $S_u$ ,  $S_h$ , and  $S_{w_j}$  account for the exchange of mass, momentum, energy, and species mass-fraction between the carrier fluid and the dispersed droplets, respectively. These terms implicitly infer the direct two-way coupling between the gas (Eulerian CFD framework) and the dispersed liquid phase (Lagrangian particles framework) considered in the present work.

For a Newtonian fluid, the shear stress tensor is given by:

$$\tau = \lambda \left( \nabla \cdot \mathbf{u} \right) \mathbf{I} + \mu \left[ \nabla \otimes \mathbf{u} + \left( \nabla \otimes \mathbf{u} \right)^T \right], \tag{5}$$

where *I* is the identity tensor,  $\lambda = -2\mu/3$  is the second viscosity coefficient given by the Stokes hypothesis, and  $\mu$  is the mixture dynamic viscosity.

The species diffusion fluxes are commonly computed using the Fickian (gradient) diffusion approximation, i.e.  $\mathbf{J_j} = \rho D_j \nabla w_j$ , where  $D_j = \mu_j/(\rho S c_j)$  is the mass diffusivity of the jth species, and Sc is the Schmidt number. The energy equation includes the interdiffusional enthalpy flux arising from the species mixing, i.e.  $\mathbf{q_d} = -\sum_{i=1}^{N_{sp}} h_i \mathbf{J_i}$ , where the enthalpy of each ith species is defined by  $h_i = e_i + p_i/\rho_i$ . No heat or mass sources are considered in the Eulerian framework in the present study, that is,  $(\hat{h})$  and  $(\hat{y})$ .

The above formulation of the governing equations represents the fully conservative 4-equation model. Equation (1) governs the evolution of the mixture density while Eq. (4) is used for the density of the first component ( $\rho_1 = \rho w_1$ ). The density of the second component is then obtained from the mixture relation  $\rho = \rho w_1 + \rho w_2$ .

Sutherland's law is employed to calculate the dynamic vis-

cosity of the dry air phase,  $\mu_1$ :

$$\mu_1(T) = \mu_{0,1} \left(\frac{T}{T_{0,1}}\right)^{\frac{3}{2}} \frac{T_{0,1} + T_s}{T + T_s},\tag{6}$$

where the free-stream values are used as the reference and the Sutherland temperature is  $T_s=110.4\mathrm{K}$  and  $\mu_{0,1}$  is the reference dynamic viscosity determined at the reference temperature  $T_{0,1}$ . The dynamic viscosity of the water vapor gas phase can be obtained using the power law:

$$\mu_2(T) = \mu_{0,2} \left( \frac{T}{T_{0,2}^{\mu}} \right)^{n_{\mu,2}},$$
(7)

where the power law parameters of the dynamic viscosity for the water vapor (gas) component are  $n_{\mu,2}=1.15$ ,  $\mu_{0,2}=1.12e^{-05}$  Pa·s and  $T_{0,2}^{\mu}=350$  K. The dynamic viscosity of the humid (mixture) multi-component gas phase can then be obtained according to:

$$\mu = \left(\sum_{i=1}^{2} \chi_i \mu_i\right) / \left(\sum_{j=1}^{2} \chi_j \phi_{ij}\right), \tag{8}$$

where  $\chi_i$  is the molar fraction of the *i*th species, and the term  $\phi_{ij}$  is given by:

$$\phi_{ij} = \frac{\left[1 + \left(\frac{\mu_i}{\mu_j}\right)^{1/2} \left(\frac{\mathcal{M}_j}{\mathcal{M}_i}\right)^{1/4}\right]^2}{\sqrt{8\left(1 + \frac{\mathcal{M}_i}{\mathcal{M}_j}\right)}},\tag{9}$$

where  $M_1 = 28.97$  moles is the molar mass of the dry air component and  $M_2 = 18.015$  moles of the water vapor.

The heat flux of the gas phase is calculated according to Fourier's Law of heat conduction, i.e.,  $\mathbf{q_c} = -\kappa \nabla T$ , where the mixture thermal conductivity is obtained as per:

$$\kappa = \left(\sum_{i=1}^{2} \chi_{i} \kappa_{i}\right) / \left(\sum_{j=1}^{2} \chi_{j} \phi_{ij}\right). \tag{10}$$

For the dry air component,  $\kappa_1 = c_{p_1} \mu_1/Pr$  is the thermal conductivity with the (laminar) Prandtl number taken equal to Pr = 0.72, where the specific heat capacity at constant pressure is  $c_{p_1} = \gamma_1 R_{s_1}/(\gamma_1 - 1)$ ,  $\gamma_1 = c_{p_1}/c_{v_1} = 7/5$  and the specific gas constant for dry air is  $R_{s,1} = R/M_{\infty}$  where  $R \simeq 8.3145 \text{ J·K}^{-1} \cdot \text{mol}^{-1}$  is the universal gas constant. The thermal conductivity of the water vapor gas phase is obtained using the power law equation:

$$\kappa_2 = \kappa_{0,2} \left( \frac{T}{T_{0,2}^{\kappa}} \right)^{n_{k,2}},\tag{11}$$

where the power law parameters of the thermal conductivity for the water vapor (gas) component are  $n_{k,2}=1.35$  and  $T_{0,2}^{\kappa}=300$  K.

PLEASE CITE THIS ARTICLE AS DOI: 10.1063/5.0272922

Preprint where  $m_f = \rho V_p$  represents the fluid mass occupied by the

## 2. Respiratory droplets (Lagrangian)

Airborne respiratory droplets are modeled as liquid water particles in the Lagrangian frame of reference, with a twoway coupling (Eulerian-Lagrangian coupling) and a quasisteady mass transfer model for the evaporation of liquid droplets. The two-way CFD-Lagrangian particle tracking framework used in the present study was also previously assessed and validated in Lappa, Drikakis, and Kokkinakis

When the conservation equation of momentum for a particle is expressed within the Lagrangian framework, the change in momentum is balanced by the surface and body forces acting upon the particle:

$$m_d \frac{d\mathbf{u}_d}{dt} = \sum_{k=1}^n \mathbf{F}_k,\tag{12}$$

where  $m_d$  is the mass of the droplet (of diameter  $d_d = 2r_d$ ), n is the number of forces and k is an index used to indicate the generic force. In the present study, we consider the (i) drag force  $\mathbf{F}_d$ ,  $(k \equiv d)$ , (ii) pressure gradient force  $\mathbf{F}_p$   $(k \equiv p)$ , (iii) gravity force  $\mathbf{F}_g$  ( $k \equiv g$ ), and (iv) virtual mass force  $\mathbf{F}_{vm}$ ,  $(k \equiv vm).$ 

The drag force,  $\mathbf{F}_d$ , calculates the force acting on a material particle due to its velocity relative to the continuous phase, or the slip velocity,  $\mathbf{u}_s$ , based on

$$F_d = \frac{1}{2} C_d \rho A_d |\mathbf{u}_s| \mathbf{u}_s, \tag{13}$$

where  $C_d$  is the drag coefficient,  $\mathbf{u}_s = \mathbf{u} - \mathbf{u}_d$  is the droplet slip velocity, and  $A_d = \pi r_d^2$  is the frontal surface area of the (spherical) droplet. The drag coefficient in the above equation is a function of the small-scale flow features around individual particles. Resolving those features for thousands of particles is intractable from a computational efficiency perspective. It is common practice to obtain the drag coefficient from correlations, typically derived from experimental or theoretical studies. For the small liquid droplets in a viscous continuous phase,  $C_d$  is a function of the small-scale flow features around the individual particles, which can be derived using the correlation<sup>20</sup>:

$$C_d = \begin{cases} 24 \left( 1 + 0.15 Re_d^{0.687} \right) / Re_d, & \text{if } Re_d \le 10^3 \\ 0.44, & \text{else} \end{cases} \tag{14}$$

where  $Re_d = \rho |\mathbf{u} - \mathbf{u}_d| d_d/\mu$  is the droplet's relative Reynolds number;  $\rho$  and  $\mu$  are the density and dynamic viscosity, respectively, of the carrier phase with velocity u, which surrounds the droplet.

The net upward force due to pressure differences in the fluid, or buoyant force, is also considered. For the pressure gradient force,  $\mathbf{F}_p$ , no correlation is necessary since it depends on the droplet volume  $(V_d)$  and the gradient of the (static) pressure of the continuous phase:

$$\mathbf{F}_p = -V_d \nabla p. \tag{15}$$

The force imparted onto the droplet by an external acceleration field is given by:

$$\mathbf{F}_g = (m_d - m_f)\mathbf{f}_b,\tag{16}$$

droplet (particle) volume  $V_p$ . Lastly, the expression for the virtual mass force,  $\mathbf{F}_{vm}$ , can

be cast in compact form as follows:

$$\mathbf{F}_{vm} = C_{vm} m_f \left( \frac{\mathrm{D} \mathbf{u}}{\mathrm{D} t} - \frac{\mathrm{d} \mathbf{u}_p}{\mathrm{d} t} \right), \tag{17}$$

where  $C_{vm}$  is the virtual mass coefficient and the operator D/Dt denotes the substantial derivative.  $C_{vm} = m'_f/m_f$  is an added mass coefficient, where  $m'_f$  is the virtual mass of the fluid (displaced), and is assumed to undergo the same acceleration as the droplet. The coefficient  $C_{vm}$  is influenced by the flow regime and the geometric characteristics of the droplet. For irrotational flow around a sphere,  $C_{vd}$  is typically taken as

All droplets are assumed to be spherical such that their mass is given by  $m_d = \rho_d \pi d_d^3/6$ . The evolution of the (spherical) droplet mass,  $m_d$ , is described by the following conservation equation, the so-called Maxwell solution for evaporation of a spherical droplet<sup>21</sup>:

$$\frac{\mathrm{d}m_d}{\mathrm{d}t} = -\pi \rho D_v d_d \, \mathrm{Sh} B_M,\tag{18}$$

where  $\rho = \rho_v + \rho_g$  is the density of the mixture of vapor and air containing the droplet,  $D_{\nu}$  is the binary diffusivity of the liquid-vapor in the air, and  $B_M$  is the Spalding mass transfer number:

$$B_M = (\rho_{v,s} - \rho_{v,\infty}) / \rho_{g,s} , \qquad (19)$$

where  $ho_{\nu,s}$  is the density of the liquid-vapor (gas-phase) at the droplet surface,  $\rho_{\nu,\infty}$  is the density of the liquid-vapor in the air containing the droplet, and  $\rho_{g,s}$  is the density of the carrier mixture phase at the droplet surface. The density of the vapor at the droplet surface,  $\rho_{v,s}$ , is given by:

$$\rho_S = p \mathcal{M}_1 / R \widehat{T}_S , \qquad (20)$$

where  $\widehat{T}_S$  is the Eulerian–Lagrangian averaged temperature at the saliva droplet surface,  $\widehat{T}_S \simeq (2T + T_d)/3$ , where T is the carrier phase temperature and  $T_d$  the particle temperature.

The Sherwood number represents the ratio between the convective and diffusive mass transfer rates and is given by:

$$Sh = 2 + 0.6\sqrt{Re_d} \, Sc_{\infty}^{1/3},$$
 (21)

where the Schmidt number,  $Sc_{\infty} = v/D_{\nu}$ , represents the ratio between the viscous and mass diffusion rates, where  $v = \mu/\rho$ is the kinematic viscosity of the multicomponent (gas-phase) air mixture containing the droplet.

Regarding the droplet energy balance, the thermal gradient in the liquid phase is rather small for the conditions considered in the present work, and thus, it can be formulated as:

$$m_d C_{p,d} \frac{\mathrm{d} T_d}{\mathrm{d} t} = -\kappa A_d \frac{2(T_d - T)}{d_d} + \frac{\mathrm{d} m_d}{\mathrm{d} t} h_{fg}, \qquad (22)$$

where  $T_d$  is the droplet temperature,  $A_d = \pi d_d^2$  is the droplet surface area,  $h_{fg}$  is the specific latent heat of vaporization of

PLEASE CITE THIS ARTICLE AS DOI: 10.1063/5.0272922

Preprint 5

the liquid droplet, and  $\kappa$  is the thermal conductivity of the multi-component gas carrier phase surrounding the droplet obtained using Eq. (10).

Droplet collision, atomization, and secondary breakup are not considered because of the low particle concentration in the room.<sup>22</sup> A stick boundary condition is applied when droplets hit a solid surface, a common practice for this type and range of particle sizes in the literature. 22-24 The authors recognize that some of the particles could be reflected on solid surfaces or resuspended in the air after deposition. However, their effect on our observations would be negligible.

All liquid water droplets have a constant density of  $\rho_d$  = 997.561 kg/m<sup>3</sup>. For simplicity, the present study does not consider the effect of non-volatile compounds, such as salts and lipids, on the decrease in size of simulated airborne liquid droplets during evaporation.

# 3. Coupling terms for the Eulerian equations

The coupling terms appearing in Eqs. (1)-(4) (by which the dispersed droplets can exert a back influence on the carrier flow), can now be precisely defined:

$$S_m(i,j,k) = -\sum_{q=1}^{n} \frac{1}{dV} \frac{dm_{d,q}}{dt}$$
 (23)

$$\frac{1}{q=1} \frac{dV}{dV} \frac{dV}{dV}$$

$$\mathbf{S}_{u}(i,j,k) = -\sum_{q=1}^{n} \frac{1}{dV} \left( m_{d,q} \frac{d\mathbf{u}_{d,q}}{dt} - \mathbf{u}_{d,q} \frac{dm_{d,q}}{dt} \right)$$

$$\mathbf{S}_{h}(i,j,k) = -\sum_{q=1}^{n} \frac{m_{d,q}}{dV} C_{p,d,q} \frac{dT_{d,q}}{dt}$$
(25)

$$S_h(i,j,k) = -\sum_{q=1}^{n} \frac{m_{d,q}}{dV} C_{p,d,q} \frac{dT_{d,q}}{dt}$$
 (25)

$$S_{w_2}(i,j,k) = -\sum_{q=1}^{n} \frac{1}{dV} \frac{dm_{d,q}}{dt}$$
 (26)

where dV denotes the volume of the generic control volume CV (computational finite-volume cell), n is the number of droplets contained in said CV, and q is an index used to indicate the generic particle. The minus sign in front of each summation follows from the nature of the interphase exchange itself. For example, a decrease in the droplet liquid mass, momentum, or temperature must correspond to an increase in the carrier fluid vapor concentration, momentum, or enthalpy, respectively, and vice versa.

# B. Numerical methods

As stated in the Introduction, we consider evaporating liquid droplets expelled from a cough into the air. From a physical standpoint, the multiphase problem essentially consists of (i) a multicomponent gas (including dry air and water vapor resulting from the relative humidity of the ambient air and locally from the evaporation process of the saliva droplets) and (ii) dispersed liquid droplets. We address the gaseous phase using an Eulerian approach, while the liquid particles are addressed through a Lagrangian approach. The impact of the particles on the flow is taken into account, including changes in mass (species), momentum, and temperature (enthalpy), leading to a two-way coupling between the two distinct frame

The simulations used the CFD code CNS3D (Compressible Navier-Stokes 3D), which employs a Godunov-type method for advective terms, solved using the Riemann problem. CNS3D supports Reynolds-Averaged Navier-Stokes (RANS), Implicit Large Eddy Simulation (ILES), and Direct Numerical Simulation (DNS). 25,26 In this paper, we have used the ILES framework.<sup>27</sup> ILES in CNS3D has been extensively validated in several cases previously published.1

In the context of classical large-eddy simulations (LES), the smallest scales of turbulence, which impose the most significant computational burden, are eliminated through a lowpass filtering operation applied to the Navier-Stokes equations. The influence of these unresolved small-scale turbulent motions is then considered using subgrid-scale models. In contrast, implicit Large Eddy Simulations (ILES) rely on the computational grid as the filter, effectively removing the small unresolved scales. The modeling of these unresolved scales is then achieved implicitly through the inherent nonlinear dissipation properties of the high-resolution high-order numerical schemes employed to discretize the convective terms of the governing equations. A substantial body of literature, encompassing theoretical analyses and numerical validations, elucidates the principles of ILES methods and demonstrates their accuracy in capturing the behavior of turbulent flows.

Regarding the numerical methods utilized in CNS3D, the "Harten-Lax-van Leer-contact HLLC" approximate Riemann solver<sup>34</sup> is used to calculate the fluxes at the finitevolume cell interfaces. A one-dimensional swept unidirectional stencil is used for spatial reconstruction. Reconstruction of flow variables at cell interfaces is performed using an enhanced 11th order weighted essentially non-oscillatory (WENO) scheme<sup>25</sup> that can handle low-Mach number flows better than Monotonic Upstream-centered Scheme for Conservation Laws (MUSCL) schemes.<sup>28,35</sup> Higher-order methods provide improved accuracy and scale well across large compute systems

Moreover, phase/component variables are reconstructed following<sup>36</sup> to avoid spurious numerical oscillations<sup>37</sup> from occurring at interfaces between fluids of different heat capacity ratios  $(\gamma_i \neq \gamma_i)$  due to the use of the four-equation model; the fully conserved four-equation multi-component model described by Eq. (4) is considered a diffuse interface method<sup>17</sup> Viscous terms are solved using a standard fourth-order central scheme. Finally, the solution is advanced in time using a five-stage fourth-order Runge-Kutta method.

# C. Cruiser cabin configuration

The present study utilizes computational fluid dynamics to investigate the transmission of an airborne disease via respiratory droplets produced during coughing in a typical passenger cabin onboard a cruise ship. Figure 2 illustrates the general configuration considered and simulated. The doors leading to the toilet/shower compartment and the hallway are assumed

PLEASE CITE THIS ARTICLE AS DOI: 10.1063/5.0272922

Preprint 6

to be closed. The former leads to an asymmetry in the geometry of the cabin room and, thus, in the air flow circulation that develops. The effect of door openings between separate compartments of the cabin and ship is not considered in the present study, as its effect of the spread of the ejected airborne droplets is relatively weak, assuming that no air currents are developed due to open cabin room windows, etc. Similar scenarios can occur in other commercial environments, such as hotels, hospitals, and office blocks.

### 1. Computational domain

The temperature of a cruiser cabin, with dimensions of  $5.8 \times 2.25 \times 2.22$  m³ (length × height × width), is controlled by an a/c. The unit is placed in the center of the ceiling. It comprises a square outlet (44 cm²) and four rectangular inlets (44 × 4 cm² each), "pushing" cold air at 18 °C. Based on the AC inlet height (4 cm) and inlet airflow velocity (1.14 m/s), the inlet Reynolds number is  $Re_j \simeq 3,135$ .

The geometry is discretized using a structured orthogonal mesh composed of hexahedral elements measuring 2 cm in each direction, resulting in a mesh of approximately 3.2 million cells. The same mesh resolution has been used in previous recent studies<sup>39-42</sup> carried out using the same numerical framework and was shown to be sufficiently accurate for the purposes and scope of the present investigation, e.g., not examining turbulent flow intricacies and characteristics arising from the suddenly expanded turbulent jet flows. Regarding the present test case, we found that doubling the mesh resolution resulted in a difference of less than 7% during the first 60 s of the flow for properties such as mean flow temperature and relative humidity, while increasing the computational cost by over an order of magnitude. Conversely, halving the mesh resolution in each direction caused such flow properties to deviate by more than 12%. We used the present resolution to keep the computational cost of the current parametric study, which simulates over 2 minutes of flow, within a reasonable

Comparative analyses of implicit and explicit LES modeling approaches, using identical numerical methods and computational grids, demonstrate that the ILES exhibits significantly reduced dissipative characteristics. 43 The experimental configuration in the present study operates under the assumption that the flow emerging from the jet inlets is laminar. Consequently, the free-shear mixing layer(s) breakdown is expected to proceed more slowly and manifest itself at larger scales. The fine-scale turbulence that subsequently develops is not directly resolved, as this approach would impose prohibitively high computational demands. Moreover, the strength of these smaller, unresolved scales progressively attenuates, thus exerting an increasingly weaker influence on the overall flow dynamics and the airborne droplets, relative to the larger, resolved vortices. It is important to emphasize that the main objective of the current investigation is not to perform a detailed examination of the turbulence properties within the free shear layer(s), but rather to evaluate the effect of the developed air circulation on the transmission of airborne respiratory droplets.

# 2. Multiphase and multicomponent cough modeling

The flow field was allowed to develop for 240 s (four minutes) before coughing. The first person coughing is near the hallway, while the second occupant is at the opposite end of the cabin, as illustrated in Figs. 2 and 3. The center of the mouth in the case of cough 1 is located at (x,y,z) = (1.32, 1.63, 1.67), while that of cough 2 is located at (x,y,z) = (5.2, 1.63, 1.02). In both cases, the coughs occur along the *x*-axis, in the direction facing the other occupant. The air expelled is assumed to be at 34 °C and has a relative humidity RH = 100%. A stronger cough with a velocity of 20 m/s was considered as the worst-case scenario.

The mouth of the cough is simulated as a rectangular inlet with a width and height of approximately 40 mm and 5 mm, respectively. The duration of the cough was set to 0.12 s. and the number of particles introduced during this time varied linearly. The initial total mass of the droplets injected into the domain is 7.7 mg, resulting in approximately 20,000 droplets per cough.<sup>48</sup> The respiratory droplets are introduced evenly and randomly into the domain at the same speed as the air expelled. In addition, the particles are given a y and z velocity component and enter the airflow at a maximum angle of  $45^{\circ}$  from the centerline along the x-axis. Although the angle can vary with sex and other factors, the chosen angle represents a reasonable value reported in experiments 47,49. The angle and the (y,z) velocity components are randomly set using a pseudorandom algorithm, ensuring that the initial velocity magnitude remains the same for all droplets. Finally, a stick condition is imposed for the particles on the wall or the floor surface.

Using computational fluid dynamics simulations, it was shown that respiratory particles could travel beyond the 2 m rule and even exceed 6 m in the presence of air currents. Although the distance traveled by airborne respiratory droplets increased significantly, the vast majority fell below the head height of the person coughing at 6 m when the freestream velocity was 4 km/h ( $\approx 1.11$  m/s), meaning that the risk of directly inhaling contaminated respiratory droplets is somewhat reduced at such distances. The present study considers a moderate distance of approximately 4 m between the two cabin occupants, approximately twice the generally accepted consensus value of 2 m for the distancing policy.

The computational fluid dynamics (CFD) methods and code employed in the present study have been thoroughly validated. Specifically, multicomponent mixing models have been validated in references <sup>36,50,51</sup>, while aspects of the accuracy and performance of high-order implicit large-eddy simulations are covered in <sup>26,28,35,52–54</sup>. Furthermore, the multiphase Lagrangian-Eulerian implementation for simulating the evaporation and transmission of liquid-phase droplets within a multicomponent humid air gas phase was investigated for a reference case of single-droplet evaporation across a range of relative humidity and temperatures. Compared with previously reported results <sup>55</sup> using different numerical methods

PLEASE CITE THIS ARTICLE AS DOI: 10.1063/5.0272922

Preprint

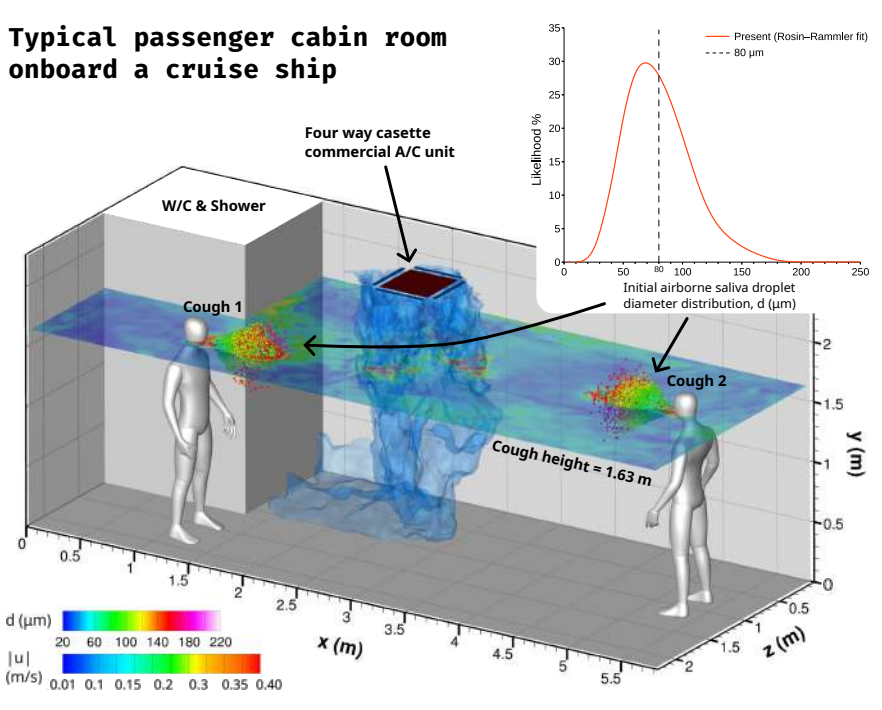


FIG. 2. Three-dimensional illustration of the dispersion of airborne respiratory droplets inside a typical passenger cabin onboard a cruise ship. The air flow circulation is developed for 2 min after the a/c unit is switched on. The blue-colored isosurfaces indicate the cold air from the a/c unit entering the room. The 2D plane at y = 1.63 m from the ground is at the same height as the mouth(s) and shows the velocity magnitude of the air. The spherical particles represent the airborne respiratory droplets, colored by their diameter, 0.15 s after the coughs.

and CFD code (specifically OpenFOAM), the error on the same grid was less than 5%. Slight differences between different CFD codes are expected due to differences in the numerical methods employed, particularly in the Eulerian finite-volume solver. The extensive numerical validation, along with the mesh resolution investigation mentioned in the previous section, guarantees the fidelity of the present simulations.

# 3. Initial droplet size distribution

The experimental measurements separately quantified the mass and number of exhaled droplets resulting from talking and coughing. Furthermore, the size distribution of the droplets was corrected near the origin of the ejection, which had been underestimated in previous studies. Fig. 8 The correction introduced was based on the dispersal analysis of the droplets, which accounts for the larger droplets dispersing into progressively smaller ones as they moved away from the origin of the mouth jet. The distribution corresponds to a fitting of the experimental data using the Rosin–Rammler distribution law also known as the Weibull distribution of 1.

The Weibull distribution effectively models the distribution of cloud droplets, including water and water-like droplets. <sup>62</sup> Some theoretical background on aspects of respiratory droplet distribution has been previously reviewed in the literature. <sup>63</sup>

The droplet size distribution adopted in the present study is obtained by the probability density function, f, using the Weibull distribution:

$$f(d_d) = \frac{n}{\overline{d}_d} \left(\frac{d_d}{\overline{d}_d}\right)^{n-1} e^{-(d_d/\overline{d}_d)^n}$$
 (27)

The fitting parameters employed in Eq. (27) and plotted in Fig. 2 are n=8,  $\overline{d}_d=80~\mu\text{m}$ , while  $d_d$  is the range of diameters of the spherical droplet particles considered (here  $d_d \in [5,300]$ ). Note that to obtain the percentage of likelihood, the probability density function, f, must be normalized by its sum, i.e.,  $f(d_d)/\Sigma_{d=5}^{300}f(d_d)$ .

# 4. Initial and boundary conditions

The air is modeled as a two-component gas (miscible) mixture comprising dry air and water vapor. The chosen values

PLEASE CITE THIS ARTICLE AS DOI: 10.1063/5.0272922

<u>Preprint</u> 8

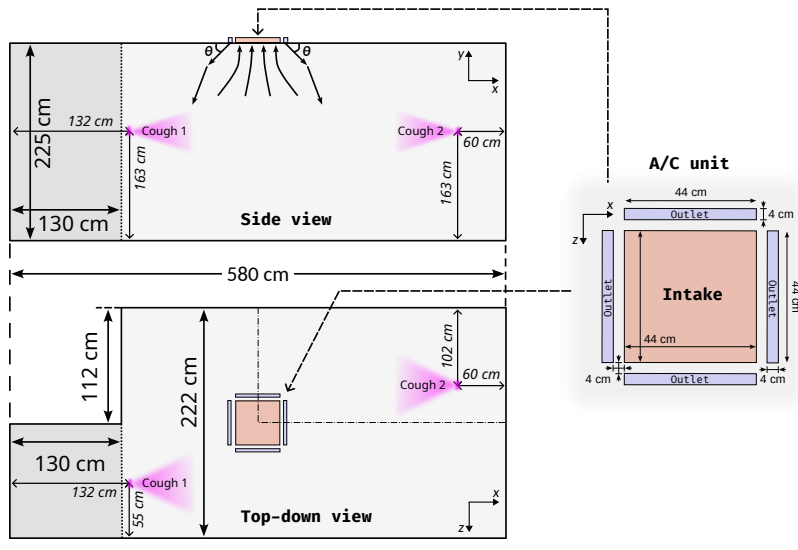


FIG. 3. Sketch illustrating the size and location of the commercial four-way square cassette a/c unit and the location of the two coughs. The present study examines two inflow angles of  $\theta=45^{\circ}$  and  $75^{\circ}$  degrees.

are typical of those measured on board cruise ships<sup>64</sup> in passenger cabins during normal operating conditions. The initial ambient room air temperature is 25 °C with a relative humidity of 60%. The simulation considers a binary multicomponent flow, such that the component mass fractions of the binary (two-component) mixture obey  $w_1 + w_2 = 1$ , where the values of  $w_1$  and  $w_2$  depend on the properties of the air, i.e., the relative humidity and temperature. The first component is dry air (0% moisture) with an adiabatic index of  $\gamma_{da} = 7/5$  and a molar mass of  $\mathcal{M}_{da}=28.964$  kg/kmol. The second component is water vapor with an adiabatic index of  $\gamma_{wv} = 4/3$  and a molar mass of  $\mathcal{M}_{wv} = 18.015$  kg/kmol. The mass fraction of water vapor in the ambient air and the air discharged from the air conditioning unit is carefully calibrated to achieve the desired levels of relative humidity. The observed difference in relative humidity between the ambient air in the room and the cooler air expelled by the air conditioning unit is primarily attributed to condensation within the a/c/ unit itself. This process leads to significant variations in the fraction of water vapor mass between the two air streams.

The velocity is initially assumed to be equal to zero everywhere in the room. The pressure varies in the normal (y) direction due to gravity, i.e.,

$$p(y) = p_0 + \rho g_y y , \qquad (28)$$

where the gravitational acceleration of Earth is taken as  $g_y = -9.81 \text{ m/s}^2$ . The internal energy,  $e_i$  is calculated according to:

$$e_i = (p_{da} + p_{wv})/(\gamma - 1)$$
 (29)

where  $p_{da}$  is the room pressure of the dry air component and

 $p_{wv}$  is the water vapor pressure. The former is obtained according to  $p_{da}=p_0-p_{wv}$ , where  $p_0$  here is taken to be the stagnation pressure at the ground/sea level, i.e.,  $p_0=1$  atm. The water vapor pressure is calculated according to  $p_{wv}=x_{wv}$   $p_0$ , where the molar fraction is  $x_{wv}=w_{wv}$  ( $\mathcal{M}/\mathcal{M}_{wv}$ ), and the total molar mass of a miscible mixture is obtained according to:

$$\mathcal{M} = \frac{1}{\sum_{i} (w_i / \mathcal{M}_i)} \tag{30}$$

where  $w_i$  is the mass-fraction of the *i*th component. The initial air mixture density,  $\rho$ , is taken to be constant and is calculated based on the prescribed relative humidity, i.e., the fraction of water vapor and dry air:

$$\rho = \rho_1 + \rho_2 \tag{31}$$

where the individual component density is calculated from  $\rho_i = p_i / \left(R_s^i T_0\right)$ . Here,  $R_s^i$  is the specific gas constant of the *i*th component, while  $T_0$  is the initial room temperature (stagnation).

Recent CFD studies that examine the dispersion of airborne respiratory droplets on cruise ships have determined that the optimal flow rate to operate ventilation systems to minimize dispersion is around 3 ACH. 13,65 Nevertheless, higher ventilation rates of up to 15 are not uncommon, particularly during the initial operation of an a/c unit, thereby posing a greater risk of transmission. The present study considers an ACH of 11, based on the total mass flux of the a/c inlets and the dimensions of the simulated cabin (Fig. 3), resulting in an incoming

PLEASE CITE THIS ARTICLE AS DOI: 10.1063/5.0272922

Preprint 9

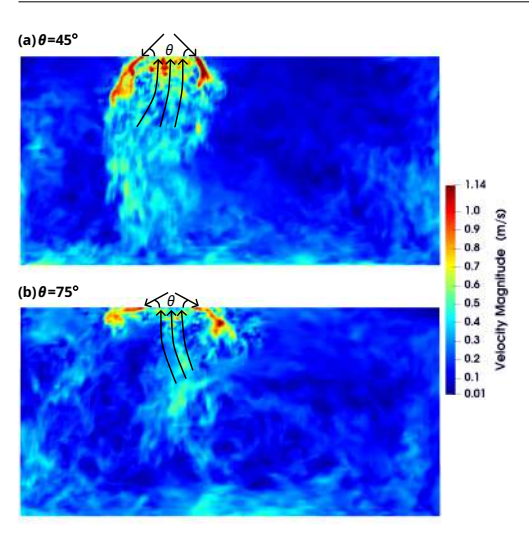


FIG. 4. Sketch illustrating the inflow angle of the cooled air from the a/c unit considered in the present study: (a)  $45^{\circ}$ , and (b)  $75^{\circ}$ . Contour surface plot on the (xy)-plane (z=111~cm) of the air velocity magnitude 240 s after the a/c unit is activated; red color indicates the maximum velocity of the air expelled by the a/c unit (1.14~m/s).

airflow speed of 1.14 m/s from the a/c inlets. Despite this modest velocity, the air currents that form in the room reach a maximum speed of  $\approx 0.3$  m/s, particularly along the surfaces of the room and in the vicinity of the a/c unit, regardless of the inlet flow angle, as Fig. 4 reveals. Nonetheless, occasional gusts of air reaching  $\approx 0.7$  m/s can still form near the a/c unit. As such, the overall effect of the developed airflow circulation on the larger and heavier airborne respiratory droplets is expected to be weak, while the dispersion of the smaller and lighter droplets remains somewhat uncertain.

Most commercial air and cooling units allow users to set the desired airflow angle. The parameters influencing this choice mainly depend on user comfort preferences and factors such as the mitigation of airborne respiratory droplets, for which limited information and guidance are available. To this end, the present study investigates whether the incoming airflow angle of a commercial four-way cassette a/c unit can affect the dispersion of airborne respiratory droplets produced from coughing within the passenger cabin, potentially increasing the risk of airborne transmission. Thus, the primary objective of this study is to provide further recommendations and guidance for the operation of a/c units in the examined or other equivalent room settings.

Initial simulations indicated that at relatively low airflow angles of  $45^{\circ}$ , the updraft produced by the column of air moving into the a/c unit bends the direction of the expelled cooled air inward and toward the centerline of the unit, as depicted in Fig. 4(a). Therefore, the second angle considered in the present study is a larger  $75^{\circ}$ , which, as shown in Fig. 4(b), is

less susceptible to the rising column of air entering the unit. The result is the formation of a drastically different air circulation pattern within the cabin, which can potentially affect the spread of airborne respiratory droplets.

Most of the cooled, heavier air expelled from the a/c in the  $45^{\circ}$  setting is directed towards the floor due to the air being drawn into the a/c unit in the center. As a result, the cooled air disperses in all directions along the floor and rises along the walls. In the case of the  $75^{\circ}$  setting, on the other hand, the air currents that have developed in the room lead most of the air expelled from the a/c unit to move towards the bottom corner of the floor at (x,z) = (130,0) cm; this can be seen in Fig. 4(b), and is also evident later in Fig. 8(f).

The transfer of heat from the human body to the environment, influenced by clothing and other factors, can generate a thermal plume that creates localized buoyancy-driven airflow near the body. This phenomenon can alter airflow patterns and has been shown to potentially influence the dispersion of aerosols and respiratory droplets during activities such as speaking, coughing, or sneezing, particularly in scenarios involving face masks. <sup>66-69</sup>

This study focuses primarily on the near-field dispersion of respiratory droplets and aerosols released during coughing. The initial movement of these particles is dominated by the high velocity and momentum associated with the cough jet. This force-driven regime overwhelms the effects of buoyancy, which are relatively weak in comparison, particularly on short timescales (milliseconds to seconds) following ejection. Therefore, the thermal plume generated by the body has minimal impact on the early spatial distribution of droplets or aerosols during this phase, and its influence was neglected in the simulations.

The potential for buoyancy effects increases over time for aerosols, which remain suspended in the air for extended periods compared to larger droplets. However, even in this case, the relative strength of the body's thermal plume compared to ambient airflow and ventilation patterns would play a decisive role in determining their transport. In typical indoor environments with active ventilation or air circulation, forced convection from these external sources is expected to dominate over natural convection driven by body heat. Since the present study focuses primarily on understanding the mechanics behind the droplets' dispersion in environments with mechanical airflow (e.g., ventilated rooms), buoyancy effects arising from the body's thermal plume were considered secondary and excluded from the present analysis.

Nonetheless, it is acknowledged that buoyancy-driven flows may influence localized aerosol behavior in quiescent environments, where ambient air currents are weak and thermal plumes become comparatively stronger. Future work could address this scenario by explicitly accounting for buoyancy effects alongside droplet evaporation and particle interactions over longer timescales, enabling a more comprehensive understanding of aerosol retention and transport under such conditions.

PLEASE CITE THIS ARTICLE AS DOI: 10.1063/5.0272922

10 Preprint

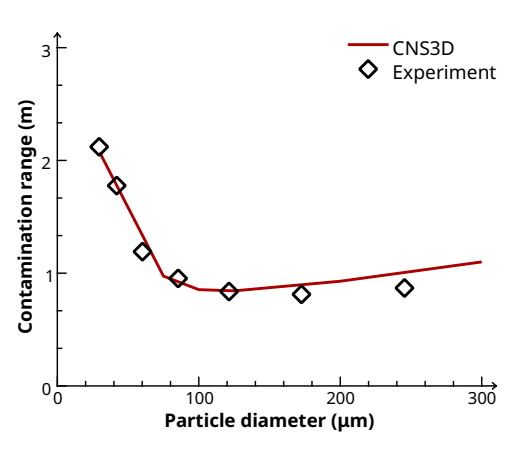


FIG. 5. Respiratory droplet contamination range (distance of deposition onto the floor) predicted by the present simulations (CNS3D method) and experiments.

# III. RESULTS

The assessment of the risk of airborne transmission is based on two primary factors: (i) the distance traveled by droplets of various sizes and (ii) the duration for which they remain suspended 1.4 meters above ground. The distance traveled indicates the expanded area subject to contamination, while the time spent above the specified height correlates with an increased window of opportunity for transmission.

The computational methodology applied to the present simulations of the droplets' motion was also evaluated by comparing the predicted trajectories that the airborne respiratory droplets follow with experimental data. 70 In this context, the contamination range is defined as the maximum ground distance achieved. Note that the contamination range is obtained here using the average of the maximum range achieved by the top 1% of the total droplets emitted to reduce uncertainty, as white noise is used to randomly perturb the inlet velocity and angle of the particles. Figure 5 illustrates that the general behavior and trend obtained from the simulations align reasonably well with the experimental reference data. The minor discrepancies observed between the numerical predictions and the experimental findings can be attributed to uncertainties likely arising from differences between the cough configuration utilized in the present numerical study and the experimental setup. 70. For example, variations in parameters such as the height and angle of the cough and the opening angle of the expelled cough cloud are potential sources of such differences. Despite these small discrepancies, both the experimental and computational findings concur that droplets measuring approximately 100  $\mu$ m in diameter exhibit the shortest contamination range.

The 1.4-meter threshold is chosen as a representative height at which an average human might inhale air contaminated with pathogen-laden airborne respiratory droplets, signifying air below the mouth that could be inhaled. It is important to note that the scope of this study is limited to aspects of airborne transmission through respiratory droplets expelled during coughing and does not encompass other potential modes of transmission.

Figure 6 illustrates the total mass of airborne respiratory droplets located above 1.4 meters from the ground, a height from which most individuals would directly inhale these droplets if within range. Furthermore, the total mass of the droplets is classified based on their diameter, enabling us to identify and determine which droplets pose the highest risk of transmission. More specifically, the total mass of the droplets is employed here as an indicator of the potential quantity of a pathogen being transported. In other words, a greater mass suggests a greater chance of transmission. Similarly, the longer a droplet remains suspended above 1.4 m, the further these droplets can potentially travel due to air circulation. The extended duration and distance traveled also indicate an increased chance of transmission and successful infection. Therefore, monitoring the location of the droplets by size category is also crucial.

Figures 7 and 8 illustrate the trajectory of airborne respiratory droplets during the 15 s following the coughs of the two cabin occupants, categorized into distinct size groups by diameter to further examine the varied spreading behavior based on the weight of the droplets. Naturally, the larger and consequently heavier droplets are expected to fall to the ground sooner; however, the size at which the smaller, and thus lighter droplets become suspended remains unclear and is chiefly determined by the strength and direction of the local airflow and the aeration formed. Even larger particles can be influenced by sufficiently strong winds, which may enable them to travel much larger distances than they would otherwise.

Figures 7(a) show the trajectory traveled by airborne respiratory droplets larger than 200  $\mu$ m in diameter. These are the most significant and heaviest saliva droplets produced during coughing. The path of these larger droplets initially follows a straight line due to their relatively large inertia, but they begin to fall rapidly once drag forces overcome their initial inertia. These heavy droplets are not influenced by air circulation and reach about a meter from the mouth in all four coughing scenarios. As expected, the duration for which the larger/heavier respiratory droplets remain above 1.4 m is the shortest according to Fig. 6, being slightly below or greater than half a second for the inflow angles 45° and 75°, respectively. Thus, large respiratory droplets above 200 um pose an immediate risk of transmission only to someone within a meter.

The next size-down category consists of respiratory droplets between 150-200  $\mu$ m in diameter. These are still considered relatively large and, as Fig. 7(b) illustrates, behave very similarly to the larger droplets above 200 μm; they initially travel in a straight line and abruptly begin to fall due to gravity once the initial inertia has been exhausted by drag forces. As mentioned above, the inflow angle of the a/c unit does not appear to cause any notable differences in spatial dispersion. At the same time, in both cases, all droplets have fallen below 1.4 m in under a second. However, statistically,

PLEASE CITE THIS ARTICLE AS DOI: 10.1063/5.0272922

Preprint 11

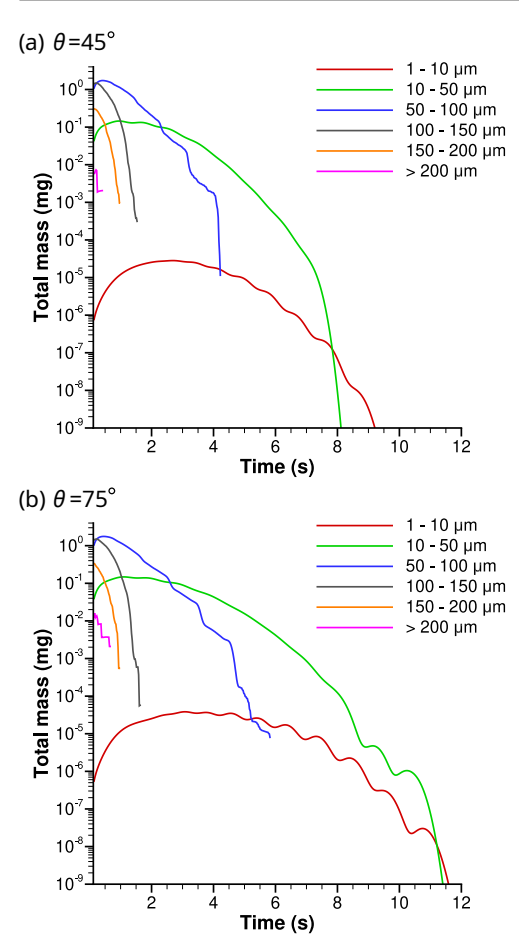


FIG. 6. Plot of the total saliva mass of the airborne respiratory droplets located 1.4 m above the floor with time, grouped into separate size ranges depending on the diameter of the (spherical) droplets, for (a)  $45^{\circ}$ -, and (b)  $75^{\circ}$ -degree a/c inlets angle.

they far outnumber the larger droplets; some can travel an additional half-meter.

The initial subtle differences in spreading behavior emerge for airborne respiratory droplets with diameters ranging from 100 to 150  $\mu m$ . For the  $45^{\circ}$  a/c inflow angle, some droplets can travel up to half a meter further, regardless of which occupant is coughing. This phenomenon is attributed to the air expelled from the a/c unit that works against the direction of the droplets in the case of the  $75^{\circ}$  inflow angle, as illustrated in Fig. 7(f). In general, droplets measuring between 100 and  $150~\mu m$  remain mostly unaffected by the air circulation within the room (approximately 0.3 m/s for the present configura-

tion), unless they interact directly with the airflow expelled from the a/c unit, which has velocities ranging from 0.7 to 1.1 m/s at the furthermost locations, as indicated in Fig. 7(f). However, in both cases of the a/c inflow angles considered, the droplets linger above 1.4 m for approximately one second, although some travel further in the case of the angle  $45^{\circ}$ .

Specifically, droplets between  $100-150\mu m$  travel almost 2 meters downstream from the cough for the  $45^{\circ}$  angle inflow, regardless of whether the occupant is coughing. This is attributed to (i) most droplets not directly interacting with the expelled air from the a/c, as Fig. 7(e) illustrates, and (ii) the relatively weak air circulation that forms in the room. In the case of cough 2, this direct interaction causes the 100 to 150  $\mu m$  droplets to travel half a meter less, only reaching up to one and a half meters from their respective cough locations.

Up to this point, the results suggest that the larger  $75^\circ$  a/c inflow angle should offer better protection against airborne transmission. However, smaller droplets can pose an equal, if not greater, risk of infection. According to the distribution of the initial particles per Eq. (27), which is fitted to experimental measurements, most saliva droplets form around the  $\overline{d}_p \simeq 80$  mum diameter. Consequently, a significant amount of ejected saliva is contained within the 50- $100~\mu$ m diameter airborne respiratory droplets. Figure 6 shows that these mediumsized droplets comprise the majority of airborne droplet mass during the first 2.5 s following the coughs, irrespective of the a/c inlet angle. Nonetheless, in the case of the  $75^\circ$  a/c inlet angle, these droplets can remain suspended above a height of 1.4 m for an additional 2 s relative to the  $45^\circ$  a/c inlet angle case, reaching nearly 6 s.

Despite the extended duration, the 50-100 µm diameter droplets remain above 1.4 m in the case of the 75° a/c inlet angle. Figures 8(a) and (b) illustrate that the spatial dispersion at the 45° angle is greater. The differences in the droplets' trajectories between the two instances are now much more anparent. This indicates that an air flow circulation of  $\approx 0.3$  m/s is only strong enough to affect the dispersion of respiratory droplets below 100 µm. A lower or higher ACH will produce weaker or stronger air circulation, affecting the droplets' size. Nonetheless, the current study unequivocally demonstrates that an ACH of 11 is adequate to influence the dispersion of airborne respiratory droplets in the crucial 50–100  $\mu$ m diameter range, which contains the largest number of initial droplets emitted during coughing (see line graph in Fig. 2), as well as a significant volume of the initial ejected saliva (see Fig. 6). Although many droplets above 100 μm may transition below 100 µm before reaching the floor, ambient air conditions that favor faster evaporation should generally lead to a faster reduction of airborne respiratory droplets.

The apparent contrast between the duration for which the droplets remain suspended above 1.4 meters and the total distance they travel highlights the underlying complexity that governs the dispersion of airborne droplets, even in this simple test case. The trajectories suggest that, in the case of the 45° inflow angle, the motion of the droplets is mainly influenced by their initial inertia and the airflow developed in the room, resulting in greater droplet dispersion. Direct interaction with air expelled from the air conditioning unit occurs

PLEASE CITE THIS ARTICLE AS DOI: 10.1063/5.0272922

Preprint 12

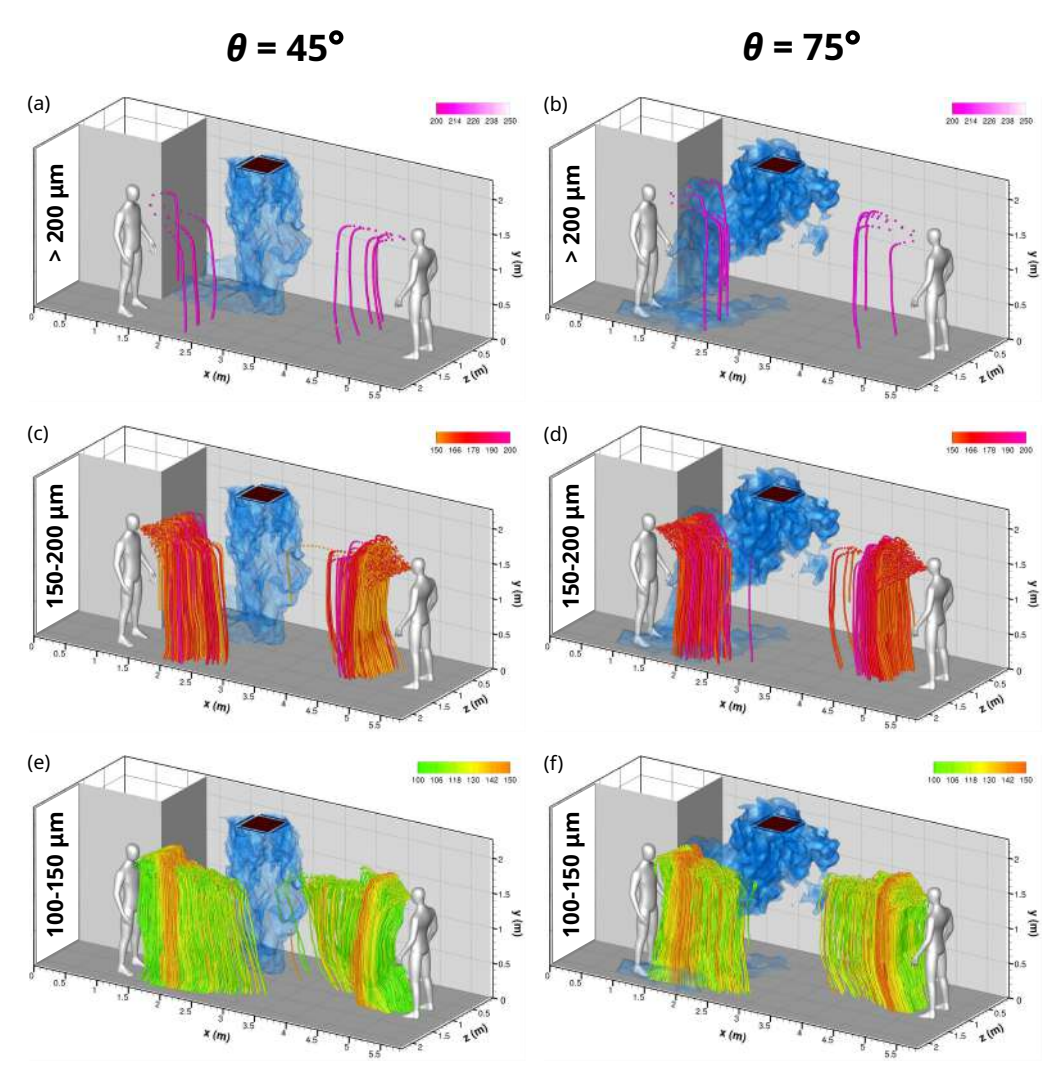


FIG. 7. Comparison of the trajectories of the airborne respiratory droplets following 15 s after the two occupants cough. The left column represents the case with an a/c inlet angle of  $45^{\circ}$ , while the right column represents an angle of  $75^{\circ}$ . The saliva droplets are categorized into distinct groups by size (diameter, d) as follows: (a)–(b)  $d > 200 \ \mu m$ , (c)–(d)  $d \in [150, 200] \ \mu m$ , and  $d \in [100, 150] \ \mu m$ .

only at the maximum distance reached, nearly 3 meters, redirecting and pushing droplets downward toward the floor. In contrast, for an inflow angle of 75° degrees, the downwash effect is weaker due to the larger angle, which reduces the rate at which droplets fall to the ground. This change in droplet behavior is further intensified by their smaller size, making them more susceptible to remaining airborne because gravitational

forces become less significant compared to the viscous drag.

Regarding the 10–50  $\mu$ m diameter droplets, the most visually striking difference between the two a/c inlet angles is the color distribution of the droplets, as indicated by the darker blue color of the trajectories in Fig. 8(c), suggesting more droplets near the lower 10  $\mu$ m range size, versus the lighter blue (cyan) trajectories in Fig. 8(d), suggesting more droplets

PLEASE CITE THIS ARTICLE AS DOI: 10.1063/5.0272922

Preprint 13

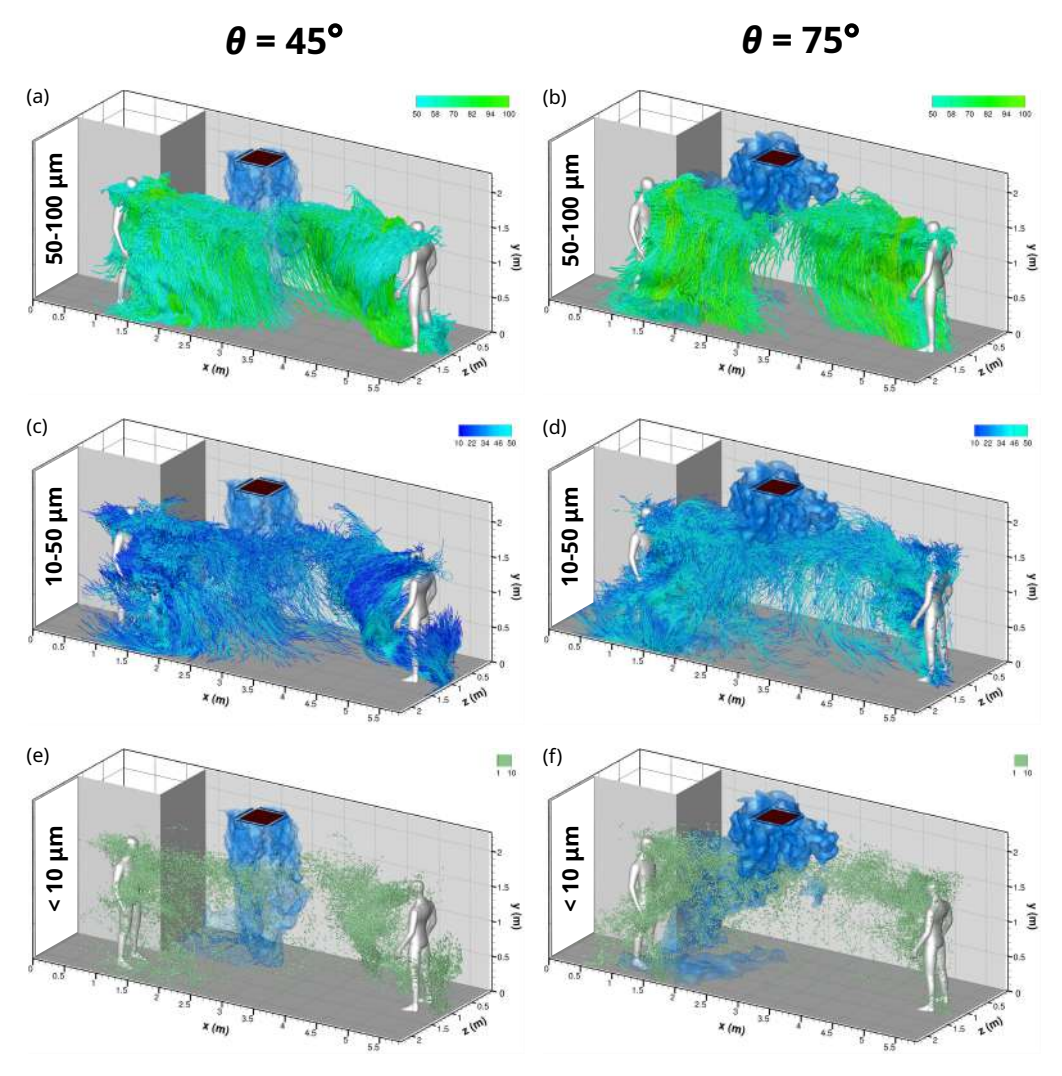


FIG. 8. Comparison of the trajectories of the airborne respiratory droplets following 15 s after the two occupants cough. The left column represents the case with an a/c inlet angle of 45°, while the right column represents an angle of 75°. The saliva droplets are categorized into distinct groups by size (diameter, d) as follows: (a)–(b)  $d \in [50, 100] \mu m$ , (c)–(d)  $d \in [10, 50] \mu m$ , and  $d < 10 \mu m$ .

near the upper 50  $\mu m$  range size. Crucially, this difference also extends far from the a/c, even near coughs; the latter implies that air circulation plays a significant role in the path that airborne respiratory droplets follow soon after being ejected. In the case of the second occupant at the far end of the room (x = 5.2 m), the air expelled from the a/c unit at an angle of  $75^{\circ}$  causes most of the smaller particles near and below  $10 \,\mu m$  in diameter to conglomerate near the body of the occupant, pushing them downward toward the wall behind. On the other hand, in the case of the 45° inlet angle, the smaller droplets appear to follow the path of some local recirculating air current. The above two observations are further corroborated by the path the smaller airborne respiratory droplets take, as seen in Fig. 8(e) and 8(f). Complete droplet dispersal reversal ocPLEASE CITE THIS ARTICLE AS DOI: 10.1063/5.0272922

This is the author's peer reviewed, accepted manuscript. However, the online version of record will be different from this version once it has been copyedited and typeset

# Preprint 14

curs in the case of the first occupant, near the hallway. The vast majority of the smaller droplets near and below 10  $\mu$  in diameter conglomerate near the body of the occupant in the case of the  $45^{\circ}$  degree a/c inlet angle, while they spread more evenly in the  $75^{\circ}$  degree case, further highlighting the complexity that governs the dispersion of the smaller respiratory droplets.

Crucially, approximately 2 to 2.5 s after the coughs, the risk of infection increases due to airborne respiratory droplets ranging between 10-50  $\mu m$  in diameter, as Fig. 6 infers. The total mass of airborne respiratory droplets above 1.4 m remains high for at least 7 s after the coughs, extending nearly to 12 s in the case of the 75° a/c inlet angle. The angle of the a/c inlet appears to promote the suspension of airborne respiratory droplets above 1.4 m and prolong the duration by an additional 4 s compared to the 45° degree angle case, an increase of almost 50%. In this case, the risk of infection from airborne respiratory droplets below 10  $\mu m$  does not appear to be significant, as most of these droplets are short-lived, as inferred by the relatively low total mass shown in Fig. 6 and in conjunction with the low dispersion observed in Figs. 8(e) and 8(f).

Regardless of the a/c inlet angle and cough location, droplets of this size can travel a maximum distance of 2 to 2.5 m from the cough, even under this relatively high ACH setting. Some droplets can travel this distance while remaining at head height by being carried by the high-speed air exhaled during a cough. This characteristic becomes noticeable at first with droplets ranging from 100 to 150  $\mu$ m in diameter, particularly for the stronger cough case simulated (20 m/s). The correlation between the increasingly larger streamwise distance traveled by the increasingly smaller airborne respiratory droplets immediately after the cough is mainly attributed to the velocity of the air expelled from the cough. The smaller and lighter particles experience a weaker gravitational pull and are more effectively convected by the high-velocity air expelled during coughing. This phenomenon applies to droplets with diameters between 50 and 100  $\mu$ m, after which the air circulation in the room begins to influence the trajectories of the smaller droplets.

It is important to note that smaller droplets, those under  $10~\mu m$  in diameter, can potentially remain suspended in the air for extended periods, even in cases of weaker air circulation than the present, such as when air conditioning operates at an air change rate (ACH) of 3 to 5. During these prolonged periods, the direct impact of the air expelled during a cough decreases, with air circulation ultimately determining the distribution of the small respiratory droplets. To provide more accurate predictions about the reach of such aerosol droplets, simulations must be tailored to the specific environments, considering unique room configurations and ventilation properties.

Although the temperature and relative humidity in a passenger cabin have been found to vary minimally compared to the values currently used 64, different conditions in other rooms or environmental settings can hinder evaporation, thereby prolonging the time it takes for smaller respiratory droplets to remain airborne and, consequently, increasing the probability

of infection. For example, relative humidity can have a particularly pronounced effect, as droplets can evaporate to their dry nuclei under sufficiently dry conditions while remaining liquid in sufficiently humid wet environments. Consequently, these tiny, lightweight droplets can be carried by air circulation over greater distances, following more complex and less predictable paths than larger airborne respiratory droplets, which may not be as straightforward or apparent as in the case of larger airborne respiratory droplets, as Figs. 7 and 8 demonstrate.

Contrary to common expectations, dry ambient conditions increased the number of airborne virus-laden nuclei by more than four times due to reduced droplet sedimentation from rapid evaporation. <sup>71–73</sup> Therefore, higher ventilation rates that prolong the time airborne droplets remain suspended can increase the risk of transmission. Fast evaporation would ensure the complete evaporation of all respiratory droplets within a time that does not allow significant dispersion (as in the present case). On the other hand, a slower evaporation rate would allow more of the larger droplets to settle onto a surface due to gravity, while also providing more time for the smaller droplets to remain airborne.

Notwithstanding other preventative measures, the present results suggest that lower ventilation rates are preferable to minimize and delay the suspension and dispersal of microdroplets and aerosols in the air circulation while a cabin is occupied. Although HVAC systems can contribute to the formation of aerosol-laden air currents, in the configurations examined here, they also acted as a barrier to dispersing larger respiratory droplets, regardless of the air conditioner inflow angle. The higher inlet angle (75°) decreased the sedimentation and airborne distance traveled by the ejected respiratory droplets. However, a smaller angle (45°) might perform better if a cough occurs nearer to, or below, the a/c unit. The time during which smaller droplets remained airborne above 1.4 meters from the ground was prolonged between 20 and 40% for droplets with diameters ranging between 1-10 and 10-50 micrometers, respectively, in the case of the higher a/c inlet angle (75°).

The preceding discussion demonstrates that droplet dispersion and subsequent viral transmission involve a complex interplay of factors. These include droplet size, virus concentration within the droplets, ambient environmental conditions, and the specific configuration of ventilation systems. Considering these factors in conjunction with general considerations of air quality is essential. A balance between measures to prevent airborne transmission and those designed to maintain passenger comfort may be needed. This balancing act should be informed by the severity of the circumstances, particularly in differentiating between normal operating conditions and periods of an ongoing airborne disease outbreak on board.

# IV. CONCLUSIONS

The present study investigated the dispersion of airborne respiratory droplets within a typical passenger cabin on a

PLEASE CITE THIS ARTICLE AS DOI: 10.1063/5.0272922

Pre
cru
pel
in t
floo
tota
rate
bie
use
ativ
240
for
I
inta
in
sm.
disi
per
per
ica
tor
sur
tras
ods

Preprint 15

cruise ship, considering two different inflow angles of air expelled from a four-way cassette air conditioning unit located in the middle of the ceiling. The AC unit was set to a mass flow rate corresponding to about 11 ACH, given the size and total volume of the cabin considered. The typical ventilation rate ranges from 1 to 15 ACH, depending on the initial ambient air properties, the number of occupants, and the desired user settings. Thus, the mass flow rate of the a/c unit was relatively modest but not atypical. The coughs are introduced 240 s (4 minutes) after the a/c unit is turned on, allowing time for the complex air circulation in the room to develop.

During a cough or sneeze, mucosalivary fluid is expelled into the air as droplets. <sup>74</sup> Typically, droplets larger than 5  $\mu$ m in diameter are termed respiratory droplets, whereas those smaller than 5  $\mu$ m are classified as aerosols. <sup>75</sup> However, this distinction is not absolute, as larger droplets can remain suspended in the air and become airborne <sup>76</sup>, for example, depending on air currents. The size of the droplets significantly influences their dispersal range. <sup>48,77</sup> Large respiratory droplets usually settle quickly and contaminate nearby surfaces, <sup>55,78</sup> posing a risk of fomite transmission. In contrast, smaller droplets can remain airborne for extended periods, posing a prolonged and long-range transmission risk. <sup>79</sup>

The results indicate that particles larger than 100 micrometers ( $\mu$ m) are not affected by air circulation, even for the modest air change per hour (ACH = 11) considered. However, even larger droplets can remain airborne at a higher operating ACH or become suspended due to strong air circulation. In the present case, all droplets exceeding 100  $\mu$ m fall below 1.4 m from the ground within 2 s after the coughs and travel no further than 2 m from the person coughing, regardless of the a/c inlet angle. This behavior is attributed to the significant inertia of large airborne respiratory droplets compared to the strength of the drag force of the airflow circulation. Generally, using a 75°-degree a/c inlet angle reduces the travel distance of larger droplets (100-200  $\mu$ m in diameter) by only about half a meter for the position of the two coughs considered.

Furthermore, the results presented indicate that air circulation patterns begin to exert a noticeable influence on the dispersion of airborne respiratory droplets with diameters smaller than 100 micrometers. Under the conditions examined in this study, small *liquid* droplets undergo evaporation within a relatively short period and over a limited distance, suggesting a reduced risk of airborne transmission associated with these droplets. However, it is crucial to acknowledge that saliva droplet remnants, which persist after evaporation, known as droplet nuclei, can still pose a non-negligible risk of transmission.

The current study does not argue against using ventilation systems while a room is occupied. In practical scenarios, higher ventilation rates are generally favorable when a room is not occupied, since increased ventilation promotes faster evaporation of droplets and more efficient air purification, thereby reducing the likelihood of fomite transmission (transmission through contaminated surfaces). However, excessively high ventilation rates during occupancy can have the unintended consequence of transmitting *lighter* airborne droplets over greater distances within the room, thus increas-

ing the risk of airborne transmission. The optimal balance between low and high ventilation rates depends on the interaction between the time the aerosols remain airborne and the distance they can travel during that time. Lower ventilation rates tend to prolong the airborne time of aerosols, while higher rates increase the distance they travel. Therefore, a lower ventilation rate might be preferable when ambient conditions, such as low humidity, promote rapid droplet evaporation, thereby eliminating all liquid aerosol droplets. Conversely, a higher ventilation rate might be more suitable in conditions where evaporation is slower, forcing smaller aerosol-borne droplets to settle on surfaces, but not so high as to prevent settling altogether or cause resuspension of settled particles.

Furthermore, this study shows that the angle at which air is introduced into the room by the HVAC system also significantly affects the aforementioned characteristics of aerosol dispersion. Compared to typical rooms in buildings, most passenger cabins on cruise ships are considerably smaller and often have a different, typically L-shaped layout, due to an en-suite bathroom. The proximity of air supply and return vents and a reduced room volume can lead to complex and potentially less predictable airflow patterns. These complex patterns can lead to the formation of "dead zones" with inadequate ventilation or areas where contaminants accumulate, resulting in higher concentrations.

# **ACKNOWLEDGEMENTS**

This paper is supported by the European Union's Horizon Europe Research and Innovation Actions program under grant agreement No 101069937, project name: HS4U (HEALTHY SHIP 4U). Views and opinions expressed are those of the author(s) only and do not necessarily reflect those of the European Union or the European Climate, Infrastructure, and Environment Executive Agency. Neither the European Union or the granting authority can be held responsible for them. The cabin details are courtesy of Celestyal Cruises. We thank Mr. Kostas Synodinos and Mr. Chrysanthos Chrysanthou for providing the drawing of the Celestyal cruiser cabin.

# DATA AVAILABILITY

The data supporting this study's findings are available from the corresponding author upon reasonable request.

# REFERENCES

- <sup>1</sup>K. Kornylo, R. Henry, and D. Slaten, "Crossing borders," Clinical Infectious Diseases **54**, v–vi (2012).
- <sup>2</sup>B. A. Muritala, A.-B. Hernández-Lara, M.-V. Sánchez-Rebull, and A. Perera-Lluna, "#CoronavirusCruise: Impact and implications of the COVID-19 outbreaks on the perception of cruise tourism," Tourism Management Perspectives 41, 100948 (2022).

accepted manuscript. However, the online version of record will be different from this version once it has been copyedited and typeset This is the author's peer reviewed,

PLEASE CITE THIS ARTICLE AS DOI: 10.1063/5.0272922

- Preprint 16 3T. Syriopoulos, M. Tsatsaronis, and M. Gorila, "The global cruise industry: <sup>28</sup>I. Kokkinakis and D. Drikakis, "Implicit large eddy simulation of weakly-Financial performance evaluation," Research in Transportation Busine nt 45, 100558 (2022). and Engineering **287**, 229 – 261 (2015). <sup>29</sup>C. Fureby and F. F. Grinstein, "Monotonically integrated large eddy <sup>4</sup>L. S. Sang, "Gastrointestinal outbreak on royal caribbean cruise sickens nearly 100 people," CBS News (2025), updated on: February 7, 2025, Accessed: 2023-10-24. <sup>30</sup>L. G. Margolin and W. J. Rider, "A rationale for implicit turbulence mod-<sup>5</sup>V. Mathai, A. Das, and K. Breuer, "Aerosol transmission in passenger car cabins: Effects of ventilation configuration and driving speed," Physics of
- <sup>6</sup>Z. Zhang, T. Han, K. H. Yoo, J. Capecelatro, A. L. Boehman, and K. Maki, "Disease transmission through expiratory aerosols on an urban cs of Fluids 33, 015116 (202
- <sup>7</sup>M. Visone, M. Lanzetta, M. Lappa, C. Lanzaro, and L. Polizio, "Threedimensional simulation of clouds of multi-disperse evaporating saliva droplets in a train cabin," Pl
- <sup>8</sup>T. Dbouk and D. Drikakis, "On airborne virus transmission in elevators and confined spaces," Physics of Fluids 33, 011905 (2021).
- <sup>9</sup>P. Azimi, Z. Keshavarz, J. Laurent, B. R. Stephens, and J. G. Allen, "Mechanistic transmission modeling of covid-19 on the diamond princess cruise ship demonstrates the importance of aerosol transmission," r
- <sup>10</sup>L. Moriarty, M. Plucinski, and e. a. Marston, B.J., "Public health responses to covid-19 outbreaks on cruise ships - worldwide," MMWR Morb Mortal
- <sup>11</sup>E. C. Rosca, C. Heneghan, E. A. Spencer, J. Brassey, A. Plüddemann, I. J. Onakpoya, D. Evans, J. M. Conly, and T. Jefferson, "Transmission of SARS-CoV-2 Associated with Cruise Ship Travel: A Systematic Review.
- <sup>12</sup>L. Huang, I. Riyadi, S.and Utama, M. Li, P. Sun, and G. Thomas, "COVID-19 transmission inside a small passenger vessel: Risks and mitigation," Ocean Engineering 255, 111486 (2022).
- <sup>13</sup>K. Ritos, D. Drikakis, and I. Kokkinakis, "Virus spreading in cruiser cabin," ics of Fluids 35, 103329 (2023).
- <sup>14</sup>ASHRAE, "ANSI/ASHRAE Standard 241-2023, Control of Infectious ," (2023)
- <sup>15</sup>Bushwick, S. and Lewis, T. and Montañez, A., "Evaluating COVID risk biles," Scientific American (2020), [Online: accessed 6-February-2025].
- 16T. Dbouk and D. Drikakis, "On respiratory droplets and face masks," ds **32**, 063303 (202
- <sup>17</sup>G. Allaire, S. Clerc, and S. Kokh, "A five-equation model for the simulation of interfaces between compressible fluids," Journal of Comp ics 181, 577-616 (2002).
- <sup>18</sup>A. W. Cook, "Enthalpy diffusion in multicomponent flows," Physics of Flu-
- <sup>19</sup>M. Lappa, D. Drikakis, and I. Kokkinakis, "On the propagation and multiple reflections of a blast wave travelling through a dusty gas in a closed Physics of Fluids 29, 033301 (201
- <sup>20</sup>L. Schiller and A. Naumann, "Ueber die grundlegenden Berechnungen bei der Schwerkraftaufbereitung," VDI Zeits. 77, 318–320 (1933).
- S. Sazhin, *Droplets and Sprays* (Springer-Verlag, London, UK, 2014).
   L. K. Norvihoho, H. Li, Z.-F. Zhou, J. Yin, S.-Y. Chen, D.-Q. Zhu, and B. Chen, "Dispersion of expectorated cough droplets with seasonal influenza in an office," Phys of Fluids 35, (
- <sup>23</sup>M. Abuhegazy, K. Talaat, O. Anderoglu, and S. V. Poroseva, "Numerical investigation of aerosol transport in a classroom with relevance to COVID-
- <sup>24</sup>M. Zhao, C. Zhou, T. Chan, C. Tu, Y. Liu, and M. Yu, "Assessment of COVID-19 aerosol transmission in a university campus food environment using a numerical method," Geoscience Frontiers 13,
- <sup>25</sup>I. W. Kokkinakis, D. Drikakis, K. Ritos, and S. M. Spottswood, "Direct numerical simulation of supersonic flow and acoustics over a compression
- <sup>26</sup>D. Drikakis, M. Hahn, A. Mosedale, and B. Thornber, "Large eddy simulation using high-resolution and high-order methods," Philosophical Tran ctions of the Royal Society A: Mathematical, Physi ences 367 2985\_2997 (2009)
- <sup>27</sup>F. Grinstein, L. Margolin, and W. Rider, eds., Implicit Large Eddy Simulaon: Computing Turbulent Fluid Dynamics (Cambridge University Press, Cambridge, 2007).

- compressible turbulent channel flow," Computer Methods in Applied Me
- simulation of free shear flows," AIAA Journal 37, 544-556 (1999),
- elling," International Journal for Numerical Methods in Fluids 39, 821–841
- <sup>31</sup>L. G. Margolin, W. J. Rider, and F. F. G. and, "Modeling turbulent flow with implicit LES," Journal of Turbulence 7, N15 (2006), https://doi.org/10.1080/14685240500331595.
- <sup>32</sup>M. Hahn and D. Drikakis, "Assessment of Large-Eddy Simulation of internal separated flow," Journal of Fluids Engineering 131, 071201 (2009)
- <sup>33</sup>B. C. Vermeire, S. Nadarajah, and P. G. Tucker, "Implicit large eddy simulation using the high-order correction procedure via reconstruction scheme," nal Journal for Numerical Methods in Fluids 82, 231-260 (2016)
- 34E. F. Toro, Riemann Solvers at d Numerical Meth n, 3rd ed. (Springer-Verlag Berlin Heidelberg, 2009).
- <sup>35</sup>P. Tsoutsanis, I. W. Kokkinakis, L. Könözsy, D. Drikakis, R. J. Williams, and D. L. Youngs, "Comparison of structured- and unstructured-grid, compressible and incompressible methods using the vortex pairing problem," n Applied Mechanics and Engineering 293, 207 - 233
- <sup>36</sup>I. Kokkinakis, D. Drikakis, D. Youngs, and R. Williams, "Two-equation and multi-fluid turbulence models for Rayleigh-Taylor mixing," Internation
- <sup>37</sup>D. Drikakis and P. K. Smolarkiewicz, "On spurious vortical structures," nal Physics 172, 309-32
- <sup>38</sup>R. Spiteri and S. Ruuth, "A new class of optimal high-order strong-stabilitypreserving time discretization methods," SIAM Journa
- <sup>39</sup>D. Drikakis, I. W. Kokkinakis, and P. Tirchas, "Sparsity and mixing effects in deep learning predictions of temperature and humidity," Phy
- <sup>40</sup>F. Sofos, D. Drikakis, and I. W. Kokkinakis, "Ultra-scaled deep learning temperature reconstruction in turbulent airflow ventilation."
- <sup>41</sup>F. Sofos, D. Drikakis, and I. W. Kokkinakis, "Enhancing indoor temperature mapping: High-resolution insights through deep learning and compu-
- 42 N. Christakis, D. Drikakis, and I. W. Kokkinakis, "Advancing understanding of indoor conditions using artificial intelligence methods," Physics
- <sup>43</sup>C. Bogey and C. Bailly, "Computation of a high Reynolds number jet and its radiated noise using large eddy simulation based on explicit filtering,
- <sup>44</sup>B. Zhao, Z. Zhang, and X. Li, "Numerical study of the transport of droplets or particles generated by respiratory system indoors," Bo
- <sup>45</sup>S. Zhu, S. Kato, and J.-H. Yang, "Study on transport characteristics of saliva droplets produced by coughing in a calm indoor environment,"
- <sup>46</sup>C. Chao, M. Wan, L. Morawska, G. Johnson, Z. Ristovski, M. Hargreaves, K. Mengersen, S. Corbett, Y. Li, X. Xie, and D. Katoshevski, "Characterization of expiration air jets and droplet size distributions immediately at the mouth opening,"
- <sup>47</sup>S. B. Kwon, J. Park, J. Jang, Y. Cho, D. S. Park, C. Kim, G. N. Bae, and A. Jang, "Study on the initial velocity distribution of exhaled air from coughing and speaking," Chemosphere 87, 1260-1264 (2012).
- <sup>48</sup>T. Dbouk and D. Drikakis, "On coughing and airborne droplet transmission
- <sup>49</sup>J. K. Gupta, C.-H. Lin, and Q. Chen, "Flow dynamics and characterization
- <sup>50</sup>B. Thornber, D. Drikakis, and D. Youngs, "Large-eddy simulation of multicomponent compressible turbulent flows using high resolution methods, 67-876 (2008), special Issue of the "Turbulence and Interaction-TI2006" Conference.
- <sup>51</sup>I. W. Kokkinakis, D. Drikakis, and D. L. Youngs, "Vortex morphology in Richtmyer-Meshkov-induced turbulent mixing," Physica D

This is the author's peer reviewed, accepted manuscript. However, the online version of record will be different from this version once it has been copyedited and typeset PLEASE CITE THIS ARTICLE AS DOI: 10.1063/5.0272922

Preprint 17

Phenomena 407, 132459 (2020).

- <sup>52</sup>M. Hahn and D. Drikakis, "Large eddy simulation of compressible turbulence using high-resolution methods," International Journal for Numerical Methods in Fluids 47, 971–977 (2005), https://onlinelibrary.wiley.com/doi/pdf/10.1002/ld.882.
- <sup>53</sup>A. Mosedale and D. Drikakis, "Assessment of very high order of accuracy in implicit LES models," Journal of Fluids Engineering 129, 1497–1503 (2007).
- <sup>54</sup>K. Ritos, I. W. Kokkinakis, and D. Drikakis, "Performance of high-order implicit large eddy simulations," Computers & Fluids 173, 307–312 (2018).
   <sup>55</sup>T. Dbouk and D. Drikakis, "Weather impact on airborne coronavirus sur-
- 55T. Dbouk and D. Drikakis, "Weather impact on airborne coronavirus sur vival," Physics of Fluids 32, 093312 (2020).
- <sup>56</sup>X. Xie, Y. Li, H. Sun, and L. Liu, "Exhaled droplets due to talking and coughing," Journal Royal Society Interface 6, 703–714 (2009).
- <sup>57</sup>J. P. Duguid, "The numbers and the sites of origin of the droplets expelled during expiratory activities," Edinburgh Medical Journal **52**, 385–401 (1945).
- <sup>58</sup>J. P. Duguid, "The size and the duration of air-carriage of respiratory droplets and droplet-nuclei," Epidemiology and Infection 44, 471–479 (1946).
- <sup>59</sup>WHO, "Roadmap to improve and ensure good indoor ventilation in the context of COVID-19," World Health Organization (2021).
- <sup>60</sup>CDC, "COVID-19 Ventilation in Buildings 2023," The Centers for Disease Control and Prevention (2023).
   <sup>61</sup>ASHRAE, "ANSI/ASHRAE Standard 62.1-2019, Ventilation and Accept-
- able Indoor Air Quality," (2019).

  62 Y. Li, P. Cheng, and W. Jia, "Poor ventilation worsens short-range airborne
- 1. Ll, P. Cheng, and W. Jia, Poor ventilation worsens short-range airborne transmission of respiratory infection," Indoor Air 32, e12946 (2022).
- <sup>63</sup>A. Kızılersü, M. Kreer, and A. W. Thomas, "The Weibull distribution," Significance 15, 10–11 (2018).
- <sup>64</sup>H. Y. W. Cheung, P. Kumar, S. Hama, A. P. M. Emygdio, Y. Wei, L. Anagnostopoulos, J. Ewer, V. Ferracci, E. R. Galea, A. Grandison, C. Hadjichristodoulou, F. Jia, P. Lepore, L. Morawska, V. A. Mouchtouri, N. Siilin, and Z. Wang, "Monitoring of indoor air quality at a large sailing cruise ship to assess ventilation performance and disease transmission risk," Science of The Total Environment 962, 178286 (2025).
- <sup>65</sup> K. Ritos, D. Drikakis, and I. W. Kokkinakis, "The effects of ventilation conditions on mitigating airborne virus transmission," Physics of Fluids 36 (2024), 10.1063/5.0185296.
- <sup>66</sup>Z. Ma, D. Zhao, C. She, Y. Yang, and R. Yang, "Personal thermal management techniques for thermal comfort and building energy saving," Materials Today Physics 20, 100465 (2021).
- <sup>67</sup>A. Joshi, A. Psikuta, M.-A. Bueno, S. Annaheim, and R. M. Rossi, "Analytical clothing model for sensible heat transfer considering spatial hetero-

- geneity," International Journal of Thermal Sciences 145, 105949 (2019).
- <sup>68</sup>G. Bagheri, O. Schlenczek, L. Turco, B. Thiede, K. Stieger, J. M. Kosub, S. Clauberg, M. L. Pöhlker, C. Pöhlker, J. Moláček, S. Scheithauer, and E. Bodenschatz, "Size, concentration, and origin of human exhaled particles and their dependence on human factors with implications on infection transmission," Journal of Aerosol Science 168, 106102 (2023).
- <sup>69</sup>K. Barari, J. Thakkar, X. A. Si, R. Hajian, and J. Xi, "Facemask vapor trapping, condensation, and thermoregulation," International Journal of Heat and Mass Transfer 234, 126080 (2024).
- <sup>70</sup>L. Bourouiba, E. Dehandschoewercker, and J. W. M. Bush, "Violent expiratory events: on coughing and sneezing," Journal of Fluid Mechanics 745, 537–563 (2014).
- 71 A. Božič and M. Kandux, "Relative humidity in droplet and airborne transmission of disease," Journal of Biological Physics 47, 1–29 (2021).
- <sup>72</sup>R. Pal, S. Sarkar, and A. Mukhopadhyay, "Influence of ambient conditions on evaporation and transport of respiratory droplets in indoor environment," International Communications in Heat and Mass Transfer 129, 105750 (2021).
- <sup>73</sup>A. Bahramian, "Influence of indoor environmental conditions on airborne transmission and lifetime of sneeze droplets in a confined space: a way to reduce COVID-19 spread," Environmental Science and Pollution Research 30, 44067–44085 (2023)
- G. Lindsley, J. S. Reynolds, J. V. Szalajda, J. D. Noti, and D. H. Beezhold, "A cough aerosol simulator for the study of disease transmission by human cough-generated aerosols," Aerosol Science and Technology 47, 937–944 (2013), pMID: 26500387.
- 75 J. Atkinson, Natural ventilation for infection control in health-care settings (World Health Organization (WHO), Geneva, Switzerland, 2009) pp. xxv, 106 p.
- <sup>76</sup>D. K. Milton, "A Rosetta stone for understanding infectious drops and aerosols," Journal of the Pediatric Infectious Diseases Society 9, 413–415
- <sup>77</sup>R. Tellier, Y. Li, B. J. Cowling, and J. W. Tang, "Recognition of aerosol transmission of infectious agents: a commentary," BMC Infectious Diseases 19, 1471–2334 (2019).
- <sup>78</sup>J. S. Kutter, M. I. Spronken, P. L. Fraaij, R. A. Fouchier, and S. Herfst, "Transmission routes of respiratory viruses among humans," Current Opinion in Virology 28, 142–151 (2018).
- <sup>79</sup>A. Fernstrom and M. Goldblatt, "Aerobiology and its role in the transmission of infectious diseases," Journal of Pathogens 2013, 493960 (2013).